

Published in final edited form as:

Hear Res. 2012 October ; 292(1-2): 14–25. doi:10.1016/j.heares.2012.07.003.

Immunogold TEM of otoconin 90 and otolin – relevance to mineralization of otoconia, and pathogenesis of benign positional vertigo

Leonardo R. Andrade^{a,b,1}, Ulysses Lins^{c,1}, Marcos Farina^b, Bechara Kachar^a, and Ruediger Thalmann^{d,*}

^aLaboratory of Cell Structure and Dynamics, NIDCD, NIH, Bethesda, MD 20892, USA

^bInstituto de Ciências Biomédicas, CCS, Universidade Federal do Rio de Janeiro, Rio de Janeiro, RJ 21941-590, Brazil

^cInstituto de Microbiologia Professor Paulo de Góes, CCS, Universidade Federal do Rio de Janeiro, 21941-590 RJ, Brazil

^dDepartment of Otolaryngology, Washington University School of Medicine, St. Louis, MO 63110, USA

Abstract

Implementation of the deep-etch technique enabled unprecedented definition of substructural elements of otoconia, including the fibrillar meshwork of the inner core with its globular attachments. Subsequently the effects of the principal soluble otoconial protein, otoconin 90, upon calcite crystal growth *in vitro* were determined, including an increased rate of nucleation, inhibition of growth kinetics and significant morphologic changes. The logical next step, ultrastructural localization of otoconin 90, by means of immunogold TEM in young mature mice, demonstrated a high density of gold particles in the inner core in spite of a relatively low level of mineralization. Here gold particles are typically arranged in oval patterns implying that otoconin 90 is attached to a scaffold consisting of the hexagonal fibrillar meshwork, characteristic of otolin. The level of mineralization is much higher in the outer cortex where mineralized fiber bundles are arranged parallel to the surface. Following decalcification, gold particles, as well as matrix fibrils, presumed to consist of a linear structural phenotype of otolin, are aligned in identical direction, suggesting that they serve as scaffold to guide mineralization mediated by otoconin 90. In the faceted tips, the level of mineralization is highest, even though the density of gold particles is relatively low, conceivably due to the displacement by the dense mineral phase. TEM shows that individual crystallites assemble into iso-oriented columns. Columns are arranged in parallel lamellae which convert into mineralized blocks for hierarchical assembly into the complex otoconial mosaic.

Another set of experiments based on immunogold TEM in young mice demonstrates that the fibrils interconnecting otoconia consist of the short chain collagen otolin. By two years of age the superficial layer of mouse otoconia (corresponding to mid-life human) has become demineralized resulting in weakening or loss of anchoring of the fibrils interconnecting otoconia. Consequently, otoconia detached from each other may be released into the endolymphatic space by minor mechanical disturbances. In humans, benign positional vertigo (BPV) is believed to result from

© 2012 Elsevier B.V. All rights reserved.

*Corresponding author. Washington University School of Medicine, 660 S. Euclid Ave., St. Louis, MO 63110, USA. Tel./fax: +1 314 367 1968. thalmannr@ent.wustl.edu (R. Thalmann).

¹These authors contributed equally.

translocation of otoconia from the endolymphatic space into the semi-circular canals rendering their receptors susceptible to stimulation by gravity causing severe attacks of vertigo. The combinations of these observations in humans, together with the presented animal experiments, provide a tentative pathogenetic basis of the early stage of BPV.

1. Introduction

Otoconia are composites of protein and calcite located in the saccule and utricle of the inner ear. Because of their high density they strongly enhance the sensitivity to gravity and linear acceleration. Otoconia are the only mammalian hard tissue mineralized by calcium carbonate, whereas the other two systems, bone and teeth, consist of calcium phosphate.

Otoconia are subject to damage by drugs, inflammation, trauma, and most importantly age-induced decalcification. Progressive demineralization with advancing age leads to degradation and fragmentation of otoconia, resulting in loss of equilibrium and susceptibility to falling and bone fracture (Agrawal et al., 2009). In order to prevent or ameliorate these pathologic processes it is essential to understand the normal mechanisms underlying formation and maintenance of otoconia.

Another pathologic entity involving otoconia is benign positional vertigo (BPV). The more prevalent type (canalithiasis) is caused by translocation of mineral particles into the semi-circular canal, the less frequent (cupulolithiasis) involves particle deposits into the cupula. In both instances the pertinent receptors become sensitive to gravity and consequently certain changes of head position frequently cause violent attacks of vertigo (Baloh et al., 1987; Epley, 1992; Welgampola et al., 2011). BPV can occur at any age but is most common in the 6th & 7th decade with strong preponderance in postmenopausal women, frequently associated with osteoporosis (Vibert et al., 2003; Jeong et al., 2009).

Early TEM and X-ray microanalytic studies indicated that otoconia are formed in the late embryonic stage. After a brief peri-natal maturation period otoconia are considered essentially stable until mid-life, when clear signs of superficial demineralization are found in human otoconia (Ross et al., 1976; Lim, 1983; Anniko et al., 1984).

Availability of scanning electron microscopy (SEM) represented an important supplementation to TEM because of its capacity of excellent visualization of the three-dimensional structure, thereby facilitating evaluation of experimental interferences and otoconial pathology. However, the internal and external organic structures of otoconia are poorly preserved in SEM and superficial dissolution of the mineral phase poses problems. These limitations were overcome by implementation of the quick-freeze/deep-etch approach, which provides an unprecedented level of morphologic preservation of both organic and inorganic matrix (Lins et al., 2000).

The obvious next step is identification of the chemical nature of the substructures in question. The first substance identified already a decade ago was otoconin 90 (OC90), the principal soluble matrix molecule, which accounts for more than 90% of the soluble otoconial protein (Wang et al., 1998; Verpy et al., 1999). OC90 contains two globular domains that closely resemble the enzyme secretory phospholipase A2 (sPLA2). Otoconin-22 (OC22), the principal soluble matrix protein of aragonitic amphibian otoconia, is another homolog of sPLA2, which contains only a single sPLA2-like domain (Pote et al., 1993). The similarity in the actions of OC90 and OC22 implies that calcitic and aragonitic otoconia share fundamental mechanisms of formation (both calcitic and aragonitic otoconia consist of calcium carbonate; however they differ in polymorph). The rigid structure of the enzyme, sPLA2 conveyed by six or seven disulfide bonds, is conserved in the otoconins and

is essential for optimal interaction of the molecule with the mineral phase (Thalmann et al., 2001; Lu et al., 2010). The molecular weight of OC90 ranges between 90 and 100 kD, about half of which is accounted for by post-translational modifications, consisting predominantly of sulfated glycosaminoglycans.

The principal scaffold protein, otolin, was partially characterized in the zebra fish (Murayama et al., 2002, 2005). Otolin is a short chain collagen with a highly interactive C1q globular domain. The mammalian ortholog was documented in mouse otoconia by several investigators (Zhao et al., 2007; Yang et al., 2011; Deans et al., 2010; Lu et al., 2010; Thalmann et al., 2011).

Subsequently, several minor otoconins were identified, including osteopontin precursor, fetuinA, sparc-like protein 1(hevin), laminin alpha3 and myosin regulatory light polypeptide 9 (Thalmann et al., 2006). Osteopontin is an essential constituent of bone, and both osteopontin and fetuin are powerful inhibitors of ectopic apatite formation (Hunter et al., 1994; Giachelli, 2005). Sparc-like protein (hevin) can in part substitute for OC90 as demonstrated in ablation studies (Zhao et al., 2007). All these “minor otoconins” are calcium-binding proteins.

Identification and partial characterization of these matrix proteins provided essential information about the overall nature and function of the molecules in question. However; this approach did not address the quintessential question of how these biomolecules control and direct formation of the mineral phase. For this purpose, (Zhao et al., 2007) resorted to ablation studies of the OC90 gene. They determined that in the absence of OC90, either no otoconia or only a small number of giant, spindle-like calcitic crystal aggregates transparent and highly susceptible to dissolution were formed. In addition, they found that the sparc-like protein compensated in part for the absence of OC90. Moreover, the principal matrix protein, otolin failed to be incorporated into the matrix demonstrating that OC90 is responsible for recruitment of otolin (Murayama et al., 2005; Zhao et al., 2007; Yang et al., 2011). The most direct approach to elucidate the role of OC90 in mineralization of otoconia was implemented by Lu et al. (2010). The authors performed *in vitro* studies on the effects of recombinant OC90 upon essential crystal growth parameters of calcite. The results highlight a multifunctional role of the molecule, including a marked facilitation of nucleation, inhibition of growth kinetics and morphologic changes, resulting in a shape typical of calcitic otoconia. Several authors demonstrated that recombinant mammalian otolin interacts with OC90 *in vitro* (Deans et al., 2010; Yang et al., 2011). Moreover, Lu et al. (2010) determined that otolin modulates the growth characteristics and morphology of calcite crystals *in vitro* and that this effect is potentiated by OC90.

These *in vitro* experiments represent an essential prerequisite for elucidation of the mechanistic basis of biomolecular control of otoconial mineralization, but do not provide information about the ultrastructural localization of the proteins in question, as well as their sites and modes of interaction with the mineral phase. In the present study we approach this question by application of immunogold TEM of OC90 in different regions of young mature mouse otoconia.

In addition, we present preliminary data on immunogold TEM of otolin in the otoconial subsurface layer and the interotoconial fibrils. The data on otolin, although still incomplete, are presented at this point already because of the crucial role the damaged fibrils are assumed to play in the pathogenesis of BPV.

The more complex patterns of otolin localization and interaction in the interior of the otoconia are presented elsewhere (Moreland et al., in preparation).

2. Materials and methods

2.1. Ultra-thin sectioning and freeze-etching

In the majority of studies 21-day-old mice or 90-day-old guinea pigs were used and sacrificed according to National Institutes of Health (NIH) guidelines under the National Institute on Deafness and other Communication Disorders animal protocol 1215-08. In the otolin experiments, ED18 mice and PN10 day as well as two-year-old mice were used. The membranous labyrinth was removed and fixed as described below. The animals were treated in accordance with The Code of Ethics of the World Medical Association (Declaration of Helsinki) for experiments involving animals.

For ultra-thin sectioning, the temporal bones were rapidly removed, immersed in 0.2% glutaraldehyde (EMS, Hatfield, PA) and 4% paraformaldehyde (EMS) in sodium phosphate buffer 0.1 M (pH 7.4) for 2 h. The membranous labyrinth was dissected with care to preserve the attachment of the otoconial membrane to the sensory epithelium. Part of the fixed samples were decalcified by using 10 % EDTA (pH 7.4) with buffered 4% paraformaldehyde at 4 °C for 24 h. Samples were cryoprotected with buffered 30% glycerol, plunge-frozen in Freon 22, freeze-substituted in 1% uranyl acetate in anhydrous methanol and embedded in Lowicryl HM20 resin. Ultra-thin sections (70 nm) were obtained with a Leica Ultracut UCT ultramicrotome (Leica Microsystems, Bannockburn, IL) using a diamond knife (Diatome, Hatfield, PA), collected on nickel grids (400 mesh) and further used for immunocytochemical and analytical experimentation.

For the freeze-etching experimentation, the temporal bones were rapidly removed, immersed in 2% glutaraldehyde in phosphate buffered saline (PBS) (pH 7.4) for 1 h and then transferred to distilled water. The utricular and saccular maculae were dissected with care to preserve the otoconial membrane on top of the sensory epithelium. After several gentle washes in distilled water, each macula was placed onto a 400 µm thick slice of Bacto-agar (Difco Laboratories, Detroit, MI), mounted on filter paper covering aluminum flat specimen holders. The specimen was quick-frozen by contact with a liquid nitrogen-cooled sapphire block of a Life Cell CF-100 quick-freezing apparatus (Research and Manufacturing Co., Tucson, AR) and promptly transferred to liquid nitrogen. The specimens were fractured at -150 °C in a Balzers BAF 301 freeze-fracture machine, etched for 10 min at -110 °C, rotary shadowed with platinum (15° angle) and carbon (90° angle). The organic material was removed using sodium hypochlorite bleach and the inorganic phase dissolved in 5% hydrochloric acid. Replicas were observed in a Leo 902 (Carl Zeiss, Oberkochen, Germany) TEM in zero-loss imaging mode, operated at 80 kV.

2.2. Immunocytochemistry

Polyclonal antibodies against a synthetic polypeptide of the N-terminal sequences of OC90 were raised in rabbits (Thalman et al., 2001) For the otolin experiments, an antibody against the same sequence segment reported by (Zhao et al., 2007) was used. For immunogold labeling of OC90 and otolin, sections were incubated in 0.1% sodium borohydride, 50 mM glycine in 0.1 M Tris-buffered/0.1 % Tween 20 (TBST) for 10 min, blocked with 10% normal goat serum (NGS) in TBST for 1 h and incubated for 2 h in primary antibody in 1% NGS/TBST. Sections were washed three times in TBST, blocked in 1% NGS/TBST for 10 min and incubated in secondary antibody goat anti-rabbit conjugated with 10 nm gold particles (dilution 1:50) (Sigma-Aldrich, St. Louis, MO) in 1% NGS/TBST, 0.5% polyethylene glycol (Sigma; 20,000 mol wt) for 1 h (Petralia and Wenthold, 1999). Sections were washed in TBST and water, stained with 1% uranyl acetate (EMS) for 20 min and observed in a Leo 902 TEM or JEOL 1010 TEM (Tokyo, Japan), operated at 80 kV.

2.3. Energy filtering electron microscopy

Energy filtering was carried out with Leo 912 equipped with an in-column Omega filter and a LaB₆ filament. A slow scan CCD camera (Proscan 14-bit) and an image analysis system (ESI Pro, SIS GmbH, Germany) were used. Elemental maps for calcium were calculated by using the three-window power law method (pre-edge: 315 and 330 eV; pos-edge: 360 eV) or white line (pre-edge: 330 eV; pos-edge: 390 eV), using an energy slit of 20 eV. For electron energy loss spectroscopy, a slit width of 3 eV and a high voltage of 120 kV were used to acquire the spectra. Because the crystalline structures could interfere with the elemental analysis due to excessive electron diffraction, the microscope goniometer was tilted.

3. Results

3.1. Structural aspects

Fig. 1a provides an overview of the otoconial complex showing typical calcitic otoconia with their rounded bodies and faceted end caps. A higher magnification deep-etch preparation shows the mosaic-like meshwork of the surface fibrils (Fig. 1b). Fig. 1c, the TEM of a longitudinal (sagittal) section of a mouse otoconium shows both the inner core and the more heavily mineralized outer cortex. High magnification imaging shows details of the fibrillar meshwork of the inner core with several small deposits of mineralized matrix (Fig. 1d). The outer cortex consists of several layers of mineralized fiber bundles, oriented parallel to the surface (Fig. 1d). The fiber bundles terminate at the otoconial end facets at an angle corresponding to the inclination of the facets with respect to the main axis (Fig. 1c).

The deep-etch preparation of a cross-fractured otoconium (Fig. 1e) exposes a series of smooth surfaces, representing preferred cleavage planes. The upper edges of these lamellae are fractured, exposing the body of the crystallites. On the right-hand side of the image, the rims of the cleavage planes exhibit sharp zigzagging patterns, representing the pointed tips of the crystallites (Fig. 1e).

The high density of mineralization of the apical otoconial region is illustrated in Fig. 1f. The figure represents an ultra-thin section demonstrating columns of iso-oriented crystallites with faintly visible pointed tips. In some instances the faceted ends are fused with each other with no apparent remnants of organic matrix. The figure also demonstrates that the individual columns are lined up in parallel to form two-dimensional laminae of crystallites.

Fig. 2a and b, respectively, are freeze-etch images and ultra-thin TEM section of the interface between inner core and outer cortex. Whereas the freeze-etch image (Fig. 2a) exhibits a rather abrupt transition, the ultra-thin section in Fig. 2b indicates that the fibrillar meshwork of the inner core is continuous with the adjacent region of the outer cortex. Several crystallites, in part fused, can be distinguished in the organic matrix. The small dark spots correspond to minute crystalline formations in the Bragg diffraction mode. Fig. 2c, a cross-section through another otoconium shows several electron-dense patches in the inner core, corresponding to regions of mineralized matrix.

The thin section in Fig. 2d shows several canals traversing the outer cortex of a decalcified otoconium. This confirms the first description by Lins et al. (2000) (Fig. 4c) using a different approach (deep-etching). It seems obvious that the canals would facilitate the exchange of structural materials from endolymph into the interior and vice versa.

The deep-etch image of a longitudinal freeze-fracture (Fig. 2e) exposes a large expanse of the inner core. The inset demonstrates several subunits of the fibrillar meshwork characterized by hexagonal geometry. A higher magnification image (Fig. 2f) shows several

regions in which the meshwork is aligned in the form of iso-oriented contiguous rows of oval/hexagonal formations (subunits of the meshwork) (see arrows).

3.2. Immunogold TEM

Incubation for gold labeling resulted in partial decalcification of the preparations, thereby facilitating access of antibody to the target molecules. To ensure that labeling was optimal, the preparations were treated with EDTA in another series. Even though the density of labeling did not increase noticeably, EDTA treatment resulted in far better definition of the contours of the fibrillar or mat-like matrix (compare Fig. 3b and c).

A longitudinal section through the outer cortex, parallel to the otoconial surface (Fig. 3a) demonstrates dense gold labeling over the entire image. The higher magnification image (Fig. 3b), demonstrates that the gold particles are for the most part arranged as straight to moderately curved rows (chains). A corresponding EDTA-treated preparation (Fig. 3c) strongly enhances the contours of the background matrix.

Fig. 3d is a higher magnification view of Fig. 1d and it is presented to serve for comparison with the EDTA-treated and gold-labeled version. The distinctly visible matrix fibrils clearly overlap with the mineralized fiber bundles shown in Fig. 3d. This implies that the fibrils represent the scaffold upon which the mineral is formed. The direction of the gold particle alignment clearly shows an analogous relationship to the matrix fibrils suggesting that gold particles are attached to the same scaffold (Fig. 3e).

Fig. 4a, a cross-section through the equatorial plane, provides an overview of the labeling patterns of the principal regions of the otoconium – inner core, outer cortex and subsurface layer. Thin-labeled beams radiate from the strongly labeled core to the periphery like spokes of a wheel, terminating in the thin but strongly labeled subsurface layer. The “spokes” are interconnected by thin concentric labeled threads which subdivide the bulk of the outer core into smaller compartments representing segments of demineralized matrix.

A high power view of the densely labeled inner core (Fig. 4b) shows that several sets of gold particles are arranged in slightly to moderately curved patterns. It is most noteworthy, however, that in several locations the gold particles are arranged in oval patterns indicated by arrows (see Section 4).

Fig. 4c represents a longitudinal/oblique section of an EDTA-treated and gold labeled otoconium, more apically located than Fig. 4a and b. Because of the EDTA treatment, the contours of the unlabeled matrix are distinctly visible. Three sets of straight duct-like cavities are delineated by the rims of the matrix, resulting in a duct-like appearance (arrows). Gold labeling is for the most part aligned with the duct-like cavities (Fig. 4c). In the more peripheral regions of the image, several sets of iso-oriented contiguous rows of oval cavities are demarcated from the matrix and in part outlined by gold particles (arrows). The shape of the oval cavities resembles that of the subunits of the typical polygonal/oval fibrillar meshwork of the inner core (Lins et al., 2000).

Analogous aligned oval/polygonal formations are distinctly visible in a deep-etch preparation (Fig. 4d) fractured in a plane similar to that of the thin section of Fig. 4c. The arrow in Fig. 4d points to a row of nine contiguous polygons. It is most noteworthy that fundamentally different technical approaches exemplified in Fig. 4c and d, respectively, provide analogous results.

Fig. 4e shows an ectopic structure resembling the inner core of a rudimentary otoconium, located in the gelatinous membrane at a considerable distance from the otoconial complex

(guinea pig). No remnants of the outer cortex can be distinguished except for a few fibrils radiating from the core to the periphery.

3.3. Electron energy loss spectroscopy (EELS)

The EELS studies are intended to demonstrate independently that the calcite crystallites develop upon an organic (protein) matrix even though the specific type of protein is not identified. To enable the EELS studies calcium and nitrogen were used as markers for calcium carbonate and protein, respectively. The experiment is based on the hypothesis that the ratio between mineral vs. organic phase should increase in line with advancing mineralization.

At an early stage of mineralization (during late development) (Fig. 5a) small electron-dense dots associated with the filaments of the outer cortex can be distinguished. Accordingly, the EELS spectrum shows that both, calcium and nitrogen, peaks are low (Fig. 5b). At the more advanced stage of mineralization (after maturation), the electron-dense areas become confluent and enlarge and thereby obscure the filaments (Fig. 5c). As expected, the calcium peak is markedly increased at this stage whereas the nitrogen peak remains unchanged (Fig. 5d).

The zero-loss image of an adult mouse otoconium shows parallel columns clearly separated by electron-lucent spaces (Fig. 5e). Elemental mapping indicates that the parallel oriented columns contain substantial levels of calcium (Fig. 5f). The image further supports an essential role of the organic matrix in formation of the crystallites.

3.4. Immunogold TEM of otolin in fibrillar elements interconnecting otoconia

Fig. 6a represents an SEM in a young mature mouse demonstrating a dense array of thin, short fibrils interconnecting adjacent otoconia. Analogous images had previously been presented in the guinea pig by Lins et al. (2000), (Fig. 3a) based on deep-etching.

In E18 mice, ample gold labeling of otolin is seen on the otoconial surface and in the subsurface layer (Fig. 6b). An analogous situation is seen in Fig. 6d, where opposing otoconial surfaces are close to each other and loaded with gold particles, yet virtually no gold particles can be detected in the interotoconial space. By contrast, in Fig. 6c, the majority of gold particles are present in the interotoconial space (17 gold particles) whereas only three or four are visible on the superficial regions of the otoconium. Many of the particles are aggregated and oriented as if intended to bridge the gap, although actual fibrils cannot be detected. Most impressive is Fig. 6e where the six visible interotoconial gold particles are arranged as pairs of triplets. The triplets cover the entire gap clearly mimicking corresponding fibrils. Documentation of the alignment of two sets of triplets interconnecting adjacent otoconia was a rare success and required a great deal of effort. Unfavorable features in attempts to document the course of an entire fibril include: (1) the small diameter of otolin; (2) use of thin sectioning TEM; and (3) orientation of the fibril with respect to the plane of section.

Consequently, the alignment of two sets of triplets in the space between adjacent otoconia (Fig. 6e), provides strong support for their nature of otoconial interconnecting elements.

Fig. 6f shows the otoconial complex of a two years old mouse. Otoconia have lost their surface fibrils and are no longer connected to each other. Moreover, they assume a vertical orientation with the tips projecting into bulk endolymph. Otoconia appear only loosely attached to the remnants of the fibrogelatinous matrix at their lower pole, and should readily pass into endolymph upon minor disturbances.

4. Discussion

4.1. General commentary

The primary purpose of the present study is to extend the possibilities opened by the deep-etch technique performed by Lins et al. (2000). This approach has provided unprecedented preservation of the soft tissue elements of otoconia, particularly the intricate meshwork of the inner core as well as the extraotoconial fibrils. The obvious next goal was identification of the chemical nature of the visualized structures. Although deep-etch provided excellent resolution of details of the soft structures of the inner core; the fine structural detail and interaction of the organic with mineral phases was not well defined in some regions of the outer cortex. This is primarily due to the unpredictability of frozen sectioning, which, as a rule, exposes predominantly favored fracture planes. Consequently, in order to identify fine structural detail of the interaction of the soft structures with the mineral phase, supplementation by thin sectioning TEM was required. For optimal structural preservation, freeze-substitution of undecalcified otoconia was used.

Since OC90 accounts for more than 90 percent of the soluble protein, it was targeted first for immunogold TEM studies. Moreover, to obtain preliminary information about the chemical composition of the fibrillar interconnections of otoconia, we initiated immunogold TEM studies of otolin – the principal scaffold protein of otoconia.

Mouse was used for the immunogold studies because of the availability of molecular data, while guinea pig, because of its larger size and ease of access, and information from previous studies was the animal of choice for other purposes. The ultrastructure between these two species is not fundamentally different.

4.2. Structural aspects

In the deep-etch study by Lins et al. (2000), young mature guinea pigs were used as experimental animals. To meet the objectives of the present study, it was essential to implement molecular biologic techniques, requiring the use of mice. To enable valid comparisons with the deep-etch profiles obtained in guinea pigs, age-matched mice were used for the immunogold TEM studies (Lins et al., 2000).

Fig. 1c represents a longitudinal section through an otoconium. Fig. 1d demonstrates the regular, slightly wavy pattern of the mineralized fiber bundles arranged parallel to the surface. The same pattern can be seen in detail in Fig. 1e. In this context, it is noteworthy that analogous preparations, gold labeled for OC90, show an alignment with the particles in a direction similar to that of Fig. 1c and d. This strongly suggests that the gold particles labeling OC90 molecules are attached to the fibrillar scaffold, to be demonstrated also in other examples.

The high density of mineralization of the apical otoconial region is illustrated in Fig. 1f. The figure represents an ultra-thin TEM section showing columns of iso-oriented crystallites. In some instances the faceted ends of the crystallites can be distinguished but, in most instances, they are fused with each other with no apparent remnants of an organic matrix. In addition Fig. 1f demonstrates that individual columns are lined up in parallel to form two-dimensional laminae of crystallites. The deep-etch in Fig. 1e shows that the sheets of crystallites are assembled into three-dimensional stacks. The resulting blocks of crystallites represent major subunits or modules in the hierarchical assembly which ultimately results in the complex mosaic of the otoconial cortex.

The concept of hierarchical assembly of otoconia was originally proposed by (Mann et al., 1983), based on high-resolution TEM studies in crushed rat otoconia. The nanocrystallites

shown in Fig. 1f (circa 80 nm) closely correspond in size and shape to those described by (Mann et al., 1983), and also resemble the shape of the two orders of magnitude larger native otoconia (averaging 10 μ). Moreover, the mentioned structures all match the morphologic features of calcite crystals grown *in vitro* upon addition of OC90 to the growth solution (Lu et al., 2010). Recent studies indicate that this process is widespread in calcium carbonate and other bio-mineral systems, including bone. It is assumed that the hierarchical assembly is directed and controlled by a specific scaffold which in vertebrates typically consists of a collagenous molecule. In gravity receptor associated calcium carbonate superstructures; the scaffold molecule in question consists of the short chain collagen otolin. Because otoconia are the result of a closely regulated directional organization, they diffract as single crystals.

The non-classical crystallization pathway is frequently associated with precipitation of an initial transient amorphous calcium carbonate phase, which spontaneously converts into the stable polymorphs aragonite or calcite (Colfen, 2010). However, on the basis of the presented studies alone, it cannot be decided whether this process is operational in otoconia. More elaborate techniques are required to answer this question. Nevertheless, no matter whether the initial phase is crystalline or amorphous, the growth kinetics are based on the same principles in either condition.

4.3. Electron energy loss spectroscopy

Electron energy loss spectroscopy was used to test the fundamental hypothesis that crystallites are formed and grow in association with an organic (proteinaceous) scaffold. As expected, at an early stage of mineralization, the spectrum shows that both the nitrogen and calcium peaks of the spectrum are low. However, at the more advanced stage of mineralization, the calcium peak is markedly increased whereas the nitrogen peak remains unchanged (Fig. 5d). This confirms in objective and quantitative terms that the crystallites grow in association with an organic (proteinaceous) scaffold, although the specific type of protein is not identified in this approach.

4.4. Immunogold TEM of OC90

Because of the extraordinarily high OC90 content of otoconia, we expected that a large proportion of the visualized organic structures would consist of or contain this protein (Lins et al., 2000) (Fig. 2a, g and h). A rather high density of label was expected since OC90 can readily be extracted from the otoconial mineral phase by means of EDTA (Wang et al., 1998). This suggests that the protein is not tightly associated with the mineral phase. Indeed, a high density of gold labeling was obtained in ultra-thin sections of mineralized otoconia in the absence of EDTA treatment. Evidently, incubation for immunogold labeling results in a sufficient level of decalcification to provide access of antibody to the target molecule.

Fig. 3a, a cortical section parallel to the otoconial surface, shows a uniformly high density of labeling in all regions of the image. At higher magnification (Fig. 3b) it is seen that the gold particles are aligned in straight to moderately curved patterns. This again implies that the OC90 molecules are attached to a scaffold of corresponding shape, generally assumed to consist predominantly of otolin (Fig. 4a), a cross-section through the equatorial plane, provides a more detailed view of the labeling patterns of the principal regions of the otoconium – inner core, outer cortex and subsurface layer. The inner core is heavily labeled and thin columns radiate to the subsurface layer. Concentric labeled rings subdivide the demineralized (empty) cortical regions into smaller compartments. The empty regions of the cortex most likely represent cross-sections of the longitudinal fiber bundles. We hypothesize that these areas are unlabeled, because, as thin sections, they do not contain sufficient antigen for recruitment of the gold particles.

Fig. 4b is a high magnification view of the strongly labeled inner core. Numerous gold particles are aligned in straight or moderately curved patterns. It is most remarkable, however, that in several places, the gold particles are arranged in oval patterns (arrows). The presence of these oval formations is not necessarily in conflict with the notion that the otolin scaffold is characterized by a hexagonal shape. Since the immunogold particles are rather bulky, their attachment to a hexagonal scaffold would be expected to round out the angles of the hexagons and thereby result in oval configurations. A hexagonal structural phenotype is considered characteristic of otolin, in analogy to the homologous meshwork-forming type X collagen of mature chondrocytes (Murayama et al., 2002; Zhao et al., 2007).

Fig. 4c represents an oblique section, more apical than the plane of section of Fig. 4b. Prior to gold labeling the preparation had been treated with EDTA and as a result, the contours of the fibrillar, mat-like scaffolding are sharply defined, resulting in a clear demarcation of a series of aligned oval cavities. The outline of the cavities is in part reinforced by gold particle patterns. The cavities resemble the shape of the subunits of the fibrillar meshwork of the inner core. It is of particular interest that a fundamentally different approach – deep-etching of a freeze-fracture through a comparable plane – reveals a pattern of aligned loop-like formations similar to those described in Fig. 4c.

It is apparent that the subunits of the meshwork of the inner core exhibit a tendency to become aligned in the more apical regions. It is likely that this directional organization is related to the high rate of mineralization of the apical regions during development. In fact, this alignment of subunits may represent a stage preparatory to formation of the duct-like structures present in the cortical layer during the developmental phase (Salamat et al., 1980, Fig. 2d and e).

It is debatable, however, whether the observed structural features relating to the developmental stage are valid, considering that the experimental animals (mice) are already mature at the time of sacrifice. Formation of otoconia and their mineralization are reported to end abruptly at birth or a few days thereafter, as demonstrated by Erway et al. (1986). It is conceivable that these apparently immature structures are frozen in time in a state of “suspended animation.” On the other hand, Verpy et al. (1999) have observed that low levels of OC90 mRNA continue to be detectable for prolonged periods of time and OC90 remains present into endolymph for several days. Several reports claim ongoing mineralization in adult animals based on positive tetracycline staining. However, the concentration of the marker most likely was excessive. Reports that otoconia are renewed in a cyclical manner (Campos et al., 1990) or that they regenerate after application of high-level streptomycin (Harada and Sugimoto, 1977) have not been confirmed independently. Considering that high levels of OC90 persist in the inner ear for only a brief period of time and that they decline sharply following birth, it is likely that incorporation of otoconin into otoconial substructures takes place only for short periods of time. Following interaction with the scaffold molecule or the mineral phase, OC90 may persist unchanged for prolonged periods of time in the absence of apparent functional activity. Clarification of the complexities involved will require targeted follow up studies.

Whereas the high density of OC90 labeling in the outer cortex can be readily explained in view of the high level of mineralization, its significance in the inner core is obscure at this point. The relatively low density of matrix in the faceted tips is presumably due to displacement by the mineral phase.

4.5. Immunogold labeling of otolin in fibrils interconnecting otoconia; relevance to pathogenesis of BPV

In early SEM studies in human temporal bones, Ross et al. (1976) described significant levels of demineralization of the superficial layer of otoconia in individuals 50 years and older. Moreover, they observed in animal experiments that the otoconial subsurface layer is particularly vulnerable to demineralization. With further advances in age, demineralization may progress to degeneration and fragmentation of otoconia, resulting in loss of equilibrium, and susceptibility to falling with bone fracture; this is the leading cause of accidental death in the elderly. Although the present study is directed at the characterization of normal otoconia, some of the observed phenomena are relevant to the understanding of the susceptibility of otoconia to demineralization. In the present context, however, we limit discussion of pathologic phenomena to experimental findings believed to be relevant to the pathogenetic basis of BPV (see Section 1).

Numerous publications concerning BPV deal with the mechanisms leading to particle translocation from bulk endolymph into the semi-circular canals, frequently leading to inappropriate mode stimulation by gravity of the receptors for angular acceleration. Consequently, certain changes in head position can lead to severe attacks of vertigo with nausea. The majority of pertinent clinical studies, as well as animal and modeling experiments, deal with this advanced stage of BPV. However the pathogenetic mechanisms underlying the early stages of BPV have attracted little attention. Our immunogold TEM studies on the distribution of otolin in the fibrillar system which interconnect otoconia, as well as their anchoring in the otoconial subsurface layer should be highly relevant to this issue.

The SEM image of Fig. 6a and a deep-etch preparation previously presented (Lins et al., 2000) demonstrate fibrillar interconnections between adjacent otoconia. These thin, straight fibrils are fundamentally different from the larger diameter and frequently globular fibrils of the gelatinous membrane and those covering much of the otoconial surface (see Fig. 1b & Lins et al., 2000).

Examination of both E18, as well as young mature mice, demonstrate localized accumulation of otolin labeled gold particles within the subsurface layer and on the surface. Moreover, several aligned doublets and occasional triplets of gold particles are visible in the narrow space between adjacent otoconia, evidently corresponding to interconnecting fibrils such as those shown in the Fig. 6a, and by Lins et al. (2000). Their role as interconnecting elements is supported by characteristic doublets or triplets of gold particles spanning in part the interotoconial space in an appropriate orientation (Fig. 6c and e). Several lines of evidence from tissue cultures of the homologous collagen type X, reinforce these concepts. It should also be noted that the entire length of a given fibril is rarely labeled because the sections are very thin and may not be covered in their entirety in the plane of section (Kwan et al., 1991).

In analogy to the observations of Ross et al. (1976) in mid-aged humans, the SEM of a two-year-old mouse shows that the otoconial surface is free of fibrils, and that otoconia project deep into the free endolymphatic space. Otoconia remain in place exclusively via loose attachment of the inferior region to the remaining fibrogelatinous phase. It is obvious that at this stage otoconia should be readily translocated into the free endolymphatic space by minimal mechanical disturbance.

The observation that the fibrils interconnecting otoconia consist of otolin is plausible from a mechanical standpoint considering the high tensile strength of collagenous molecules. Excellent material properties are necessary because of the continuous motions between

otoconia during mass movements of the complex. Gold particles are also accumulated in the subsurface layer, thereby providing firm anchoring in the mineral phase. Consequently it can be assumed that the essential pathologic process leading to idiopathic (age-dependent) BPV is likely due to demineralization of the subsurface layer, which causes loss of firm anchoring of the interconnecting fibrils.

5. Conclusion

We suggest a hypothetical concept of the pathogenesis of BPV according to the evidence provided by Ross et al. (1976) and observed in the animal experiments of the present study (Fig. 6g). Partial demineralization of the subsurface layer causes loosening of the anchoring of interotoconial fibrils; at this point the fibrils are no longer able to attach otoconia to each other. This leads to detachment of otoconia from each other ultimately resulting in their release into the free endolymphatic space, from where they can be translocated into the semi-circular canal system by well-established mechanisms. More comprehensive investigations will be required to confirm these concepts and characterize them in more detail.

Acknowledgments

We thank Dr. S. Brian Andrews from NINDS-NIH for the use of the Zeiss 912 analytical TEM. We would also like to thank Endrit Agastra for assistance with the preparation of the manuscript. This work was supported by National Institutes of Health (NIH) Intramural Research Fund Z01-DC000002-22 (B.K.), NIH awards R21DC 009320 and RO1 DC 011614 (RT), and the Brazilian Agencies FAPERJ (UL) and CNPq (MF).

Abbreviations

BPV	benign positional vertigo
OC90	otoconin 90
SEM	scanning electron microscopy
sPLA2	secretory phospholipase A2
OC22	otoconin-22
TEM	transmission electron microscopy

References

- Agrawal Y, Carey JP, la Santina CC, Schubert MC, Minor LB. Disorders of balance and vestibular function in US adults: data from the National Health and Nutrition Examination Survey, 2001–2004. *Archives of Internal Medicine*. 2009; 169:938–944. [PubMed: 19468085]
- Anniko M, Ylikoski J, Wroblewski R. Microprobe analysis of human otoconia. *Acta Otolaryngology*. 1984; 97:283–289.
- Baloh RW, Honrubia V, Jacobson K. Benign positional vertigo: clinical and oculographic features in 240 cases. *Neurology*. 1987; 37:371–378. [PubMed: 3822129]
- Campos A, Canizares FJ, Sanchez-Quevedo MC, Romero PJ. Otoconial degeneration in the aged utricle and saccule. *Advances in Otorhinolaryngology*. 1990; 45:143–153.
- Colfen H. Biomineralization: a crystal-clear view. *Nature Materials*. 2010; 9:960–961.
- Deans MR, Peterson JM, Wong GW. Mammalian Otolin: a multimeric glycoprotein specific to the inner ear that interacts with otoconial matrix protein Otoconin-90 and Cerebellin-1. *PLoS One*. 2010; 5:e12765. [PubMed: 20856818]
- Epley JM. The canalith repositioning procedure: for treatment of benign paroxysmal positional vertigo. *Otolaryngology – Head and Neck Surgery*. 1992; 107:399–404. [PubMed: 1408225]

- Erway LC, Purichia NA, Netzler ER, D'Amore MA, Esses D, Levine M. Genes, manganese, and zinc in formation of otoconia: labeling, recovery, and maternal effects. *Scanning Electron Microscopy*. 1986;1681–1694. [PubMed: 3810031]
- Giachelli CM. Inducers and inhibitors of biomineralization: lessons from pathological calcification. *Orthodontics and Craniofacial Research*. 2005; 8:229–231. [PubMed: 16238602]
- Harada Y, Sugimoto Y. Metabolic disorder of otoconia after streptomycin intoxication. *Acta Otolaryngologica*. 1977; 84:65–71.
- Hunter GK, Kyle CL, Goldberg HA. Modulation of crystal formation by bone phosphoproteins: structural specificity of the osteopontin-mediated inhibition of hydroxyapatite formation. *Biochemical Journal*. 1994; 300 (Pt 3):723–728. [PubMed: 8010953]
- Jeong SH, Choi SH, Kim JY, Koo JW, Kim HJ, Kim JS. Osteopenia and osteoporosis in idiopathic benign positional vertigo. *Neurology*. 2009; 72:1069–1076. [PubMed: 19307540]
- Kwan APL, Cummings CE, Chapman JA, Grant ME. Macromolecular organization of chicken type X collagen in vitro. *Journal of Cell Biology*. 1991; 114:597–604. [PubMed: 1860888]
- Lim DJ. Otoconia in health and disease: a review. *The Annals of Otolaryngology, Rhinology & Laryngology, Supplement*. 1983; 112:12–24.
- Lins U, Farina M, Kurc M, Riordan G, Thalmann R, Thalmann I, Kachar B. The otoconia of the guinea pig utricle: internal structure, surface exposure, and interactions with the filament matrix. *Journal of Structural Biology*. 2000; 131:67–78. [PubMed: 10945971]
- Lu W, Zhou D, Freeman JJ, Thalmann I, Ornitz DM, Thalmann R. In vitro effects of recombinant otoconin 90 upon calcite crystal growth. Significance of tertiary structure. *Hearing Research*. 2010; 268:172–183. [PubMed: 20595020]
- Mann S, Parker SB, Ross MD, Skarnulis AJ, Williams RJ. The ultra-structure of the calcium carbonate balance organs of the inner ear: an ultra-high resolution electron microscopy study. *Proceedings of Royal Society of London Series B, Biological Sciences*. 1983; 218:415–424.
- Murayama E, Herbomel P, Kawakami A, Takeda H, Nagasawa H. Otolith matrix proteins OMP-1 and Otolin-1 are necessary for normal otolith growth and their correct anchoring onto the sensory maculae. *Mechanisms of Development*. 2005; 122:791–803. [PubMed: 15905077]
- Murayama E, Takagi Y, Ohira T, Davis JG, Greene MI, Nagasawa H. Fish otolith contains a unique structural protein, otolin-1. *European Journal of Biochemistry*. 2002; 269:688–696. [PubMed: 11856329]
- Petralia RS, Wenthold RJ. Immunocytochemistry of NMDA receptors. *Methods in Molecular Biology*. 1999; 128:73–92. [PubMed: 10320974]
- Pote KG, Hauer CR, Michel H, Shabanowitz J, Hunt DF, Kretsinger RH. Otoconin-22, the major protein of aragonitic frog otoconia, is a homolog of phospholipase A2. *Biochemistry*. 1993; 32:5017–5024. [PubMed: 8494877]
- Ross MD, Peacor D, Johnsson LG, Allard LF. Observations on normal and degenerating human otoconia. *The Annals of Otolaryngology, Rhinology & Laryngology*. 1976; 85:310–326.
- Salamat MS, Ross MD, Peacor DR. Otoconial formation in the fetal rat. *The Annals of Otolaryngology, Rhinology & Laryngology*. 1980; 89:229–238.
- Thalmann I, Hughes I, Tong BD, Ornitz DM, Thalmann R. Microscale analysis of proteins in inner ear tissues and fluids with emphasis on endolymphatic sac, otoconia, and organ of Corti. *Electrophoresis*. 2006; 27:1598–1608. [PubMed: 16609936]
- Thalmann R, Ignatova E, Kachar B, Ornitz DM, Thalmann I. Development and maintenance of otoconia: biochemical considerations. *Annals of the New York Academy of Sciences*. 2001; 942:162–178. [PubMed: 11710459]
- Thalmann R, Thalmann I, Lu W. Significance of tertiary conformation of otoconial matrix proteins – clinical implications. *Acta Otolaryngologica*. 2011; 131:382–390.
- Verpy E, Leibovici M, Petit C. Characterization of otoconin-95, the major protein of murine otoconia, provides insights into the formation of these inner ear biominerals. *Proceedings of the Natural Academy of Sciences USA*. 1999; 96:529–534.
- Vibert D, Kompis M, Hausler R. Benign paroxysmal positional vertigo in older women may be related to osteoporosis and osteopenia. *The Annals of Otolaryngology, Rhinology & Laryngology*. 2003; 112:885–889.

- Wang, Y.; Kowalski, PE.; Thalmann, I.; Ornitz, DM.; Mager, DL.; Thalmann, R. Otoconin-90, the mammalian otoconial matrix protein, contains two domains of homology to secretory phospholipase A2. *Proceedings of the Natural Academy of Sciences; USA*. 1998. p. 15,345-15,350.
- Welgampola MS, Bradshaw A, Halmagyi GM. Practical neurology-4: dizziness on head movement. *Medical Journal of Australia*. 2011; 195:518–522. [PubMed: 22060084]
- Yang H, Zhao X, Xu Y, Wang L, He Q, Lundberg YW. Matrix recruitment and calcium sequestration for spatial specific otoconia development. *PLoS One*. 2011; 6:e20498. [PubMed: 21652225]
- Zhao X, Yang H, Yamoah EN, Lundberg YW. Gene targeting reveals the role of Oc90 as the essential organizer of the otoconial organic matrix. *Developmental Biology*. 2007; 304:508–524. [PubMed: 17300776]

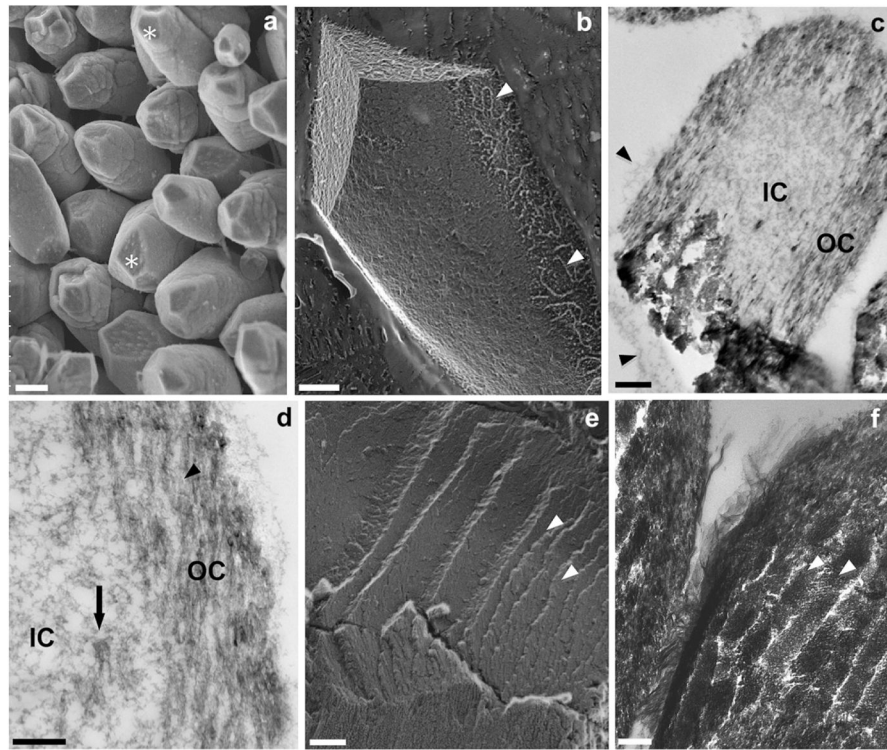


Fig 1. Fine structural features of mammalian otoconia shown by different EM techniques. (a) SEM image of adult mouse otoconia showing typical barrel-shaped morphology and faceted ends; (b) freeze-etching of guinea pig otoconium showing pointed tip and rounded bodies with abundant filaments covering the surface (arrowhead); (c) TEM of a mouse otoconium showing both outer cortex (OC) and inner core (IC); (d) corresponding high magnification image showing fibrillar meshwork of inner core (IC) with several mineralized plaques (arrow), and outer cortex (OC) with parallel aligned mineralized fiber bundles (arrowhead); (e) freeze-etch image of cross-fractured guinea pig otoconium exposing parallel-aligned lamellae consisting of fused crystallites. On the right-hand side of the image, the rims of the cleavage planes exhibit sharp zigzagging patterns, representing the pointed tips of crystallites (arrowheads); (f) ultra-thin section of the densely mineralized cortex with parallel-arranged rows of iso-oriented columns of crystallites (arrowheads). The spaces between crystallites are widened due to sectioning procedure. Bars = 2 μm (a); 1 μm (b); 0.2 μm (c), 1 μm (d), 0.1 μm (e), 0.2 μm (f).

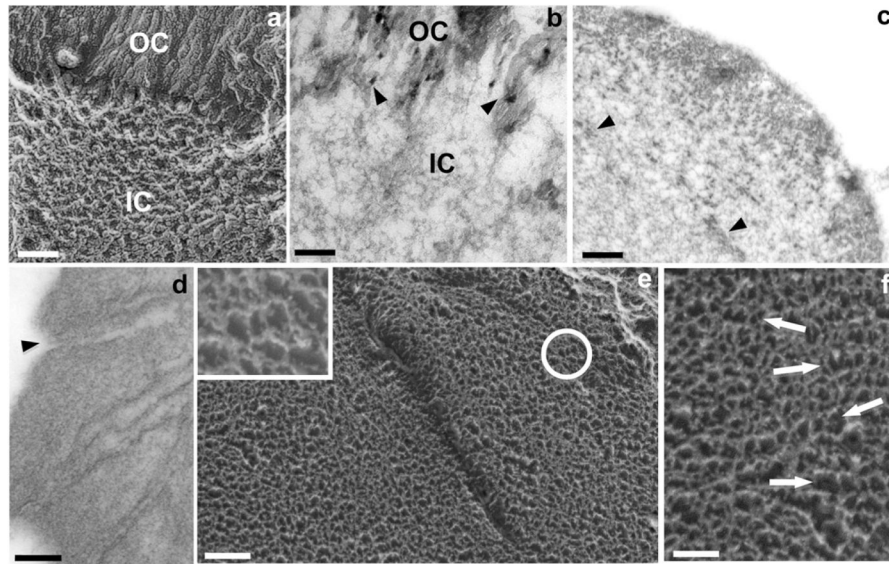


Fig 2.

Fine structural features of the inner core of mammalian otoconia demonstrated by EM techniques. (a) Freeze-etching and (b) ultra-thin sectioning TEM; (b) images of the interface between inner core (IC) and outer cortex (OC) of otoconia. The freeze-etch image (a) demonstrates a rather abrupt border, but the ultra-thin section in (b) indicates that the fibrillar meshwork of the central core is continuous with the matrix of the outer cortex. The small dark plaques (arrowheads) in the cortex correspond to crystallites in the Bragg diffraction mode; (c) cross-section of otoconium showing electron-dense spots in inner core corresponding to mineralized matrix (arrowheads); (d) EDTA-treated otoconium showing several canals traversing outer cortex, connecting otoconial surface with inner core; (e) deep-etch image of freeze-fractured guinea pig otoconium showing the dense fibrillar web of inner core and innermost region of cortex. Inset: detail of area indicated by arrow showing typical hexagonal arrangement of fibrils; (f) high magnification of inner core of guinea pig otoconium showing several rows of co-aligned polygonal formations (arrows). Bars = 0.2 μm for (a) and (b); 0.3 μm (c); 0.5 μm (d); 0.2 μm (e) and 0.08 μm (inset); 0.1 μm (f).

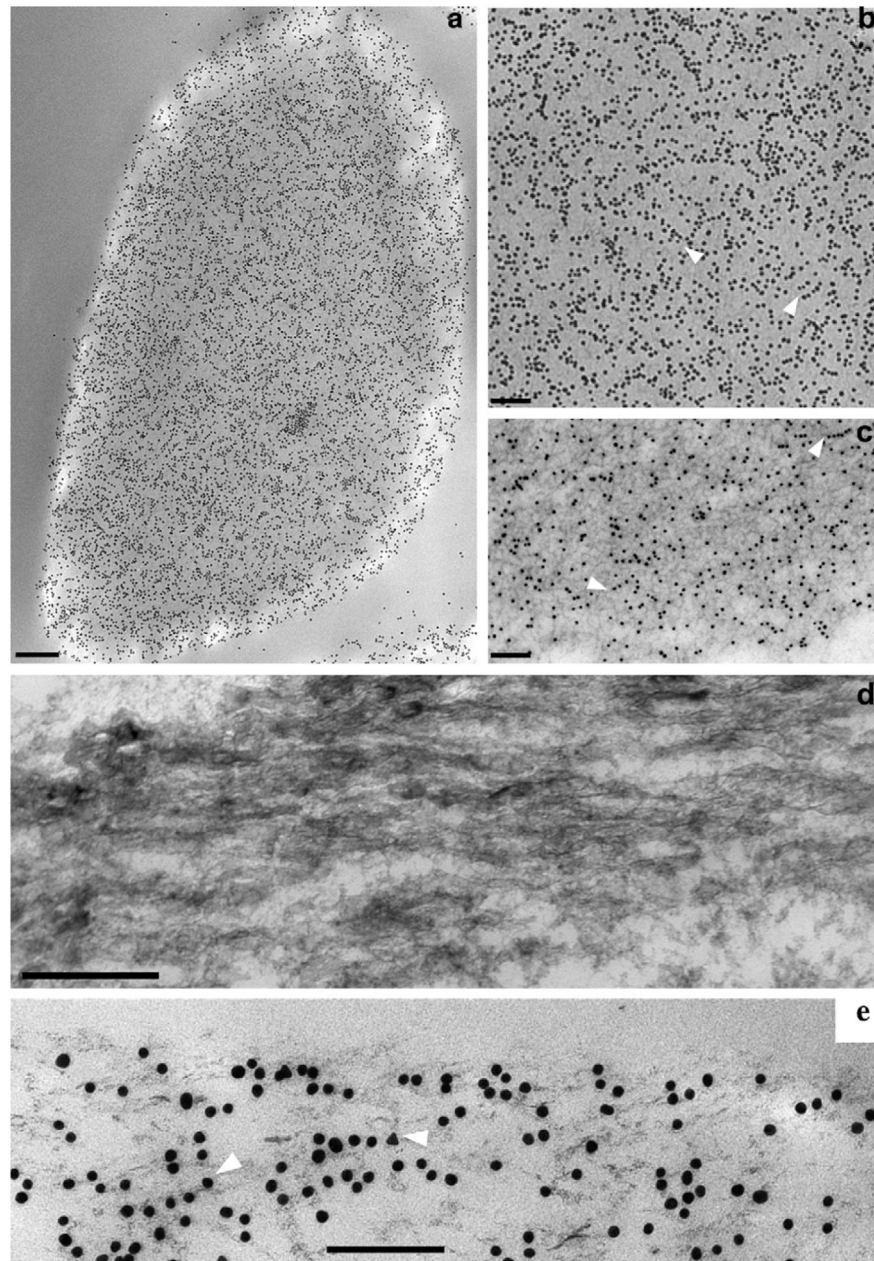


Fig 3. Immunogold TEM of OC90 in outer cortex. (a) Low magnification view of longitudinal/tangential section of outer cortex, displaying high density of gold particles; (b) high magnification of Fig. 3a, demonstrating gold particles aligned in rows in straight or slightly curved patterns (arrowheads); (c) EDTA-treated cortical region of an otoconium, distinctly showing dense unstained fibrillar matrix as well as immunogold particles. In most regions gold particles are aligned in same direction as fibrils (arrowheads); (d) ultra-thin sagittal section of outer cortex of mouse otoconium; (e) corresponding section, immunogold labeled for OC90, indicating that the majority of the particles are aligned in the same direction of mineralized fibrils shown in (d) (white arrowheads). Bars = 0.15 μm (a); 0.2 μm (b); 0.2 μm (c); 0.1 μm (d); 0.1 μm (e).

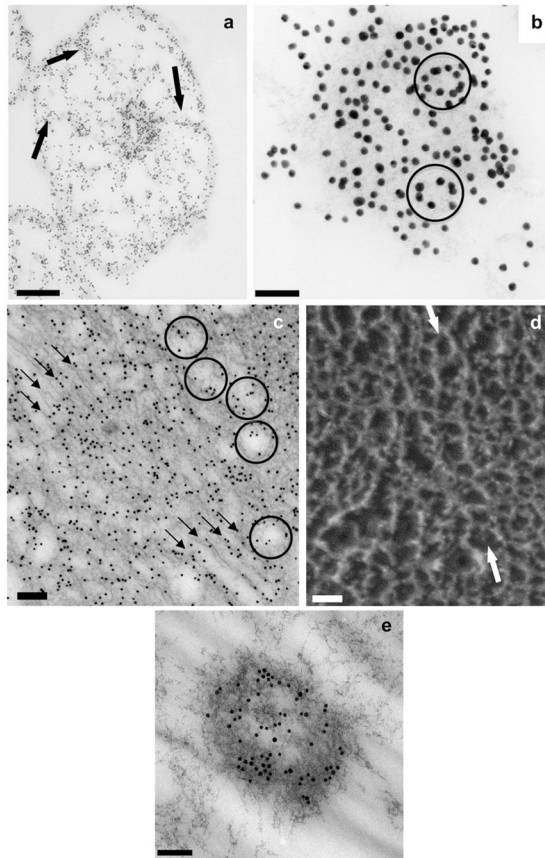


Fig 4. Immunogold TEM of OC90 and deep-etch images of otoconia. (a) Cross-section through the equatorial plane of mouse otoconium showing strongly labeled inner core. Thin spoke-like projections radiate to periphery, merging with densely labeled subsurface layer (arrows); (b) high magnification image of central core showing several oval gold particle alignments (arrows) in addition to straight or slightly curved patterns; (c) longitudinal section of an EDTA-treated gold labeled inner core. Because of EDTA treatment, the unstained matrix is sharply contoured. Three rows of gold particles in the center of image delineate sets of diagonally oriented tubular formations corresponding to cavities in the fibrillar scaffold. Several diagonally oriented contiguous, co-aligned rows of oval/polygonal fibrillar formations are seen in periphery of image (arrow); (d) deep-etch image of freeze-fractured inner core, showing several rows of oval, co-aligned fibrillar formations (arrows) analogous to those seen in the thin sectioning TEM of Fig. 4c. [Note that two totally different techniques (thin sectioning TEM and freeze fracturing) show identical patterns.] (e) ectopic immunogold labeled structure resembling inner core on an otoconium, located in gelatinous membrane. Bars = 1 μm (a); 0.05 μm (b); 0.125 μm (c); 0.05 μm (d); 0.1 μm (e).

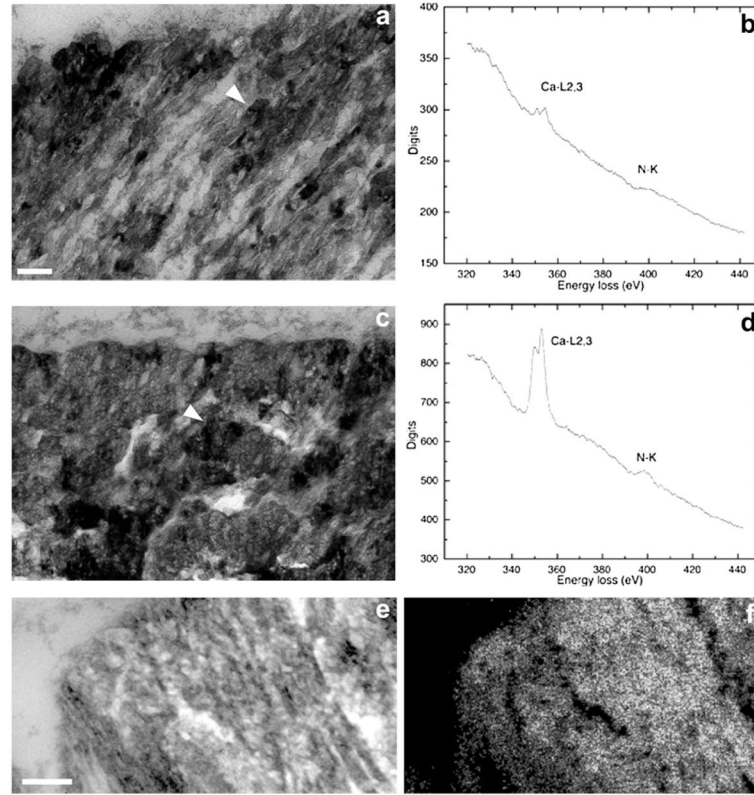


Fig 5. Analytical TEM demonstrates co-localization of mineral and organic phases. (a) TEM of the outer cortex of a mouse otoconium showing several small electron-dense mineral particles framed by fibrillar scaffolds (arrowhead); (b) electron energy loss spectrum of region indicated by arrowhead in (a), showing low peaks for both, calcium and nitrogen (markers for calcium carbonate and protein, respectively); (c) electron-micrograph of outer cortex showing a more advanced stage of mineralization than (a). The arrow points to the growing crystallites, which obscure fibrillar scaffold. The corresponding EELS shows a much higher calcium peak than (b), with the N peak unchanged (d); (e) elemental mapping of calcium of mouse otoconium in a zero-loss filtered image. Parallel columns of crystallites are separated by electron-lucent material (arrowhead); (f) calcium map of region depicted in (e). Bars = 0.1 μm for (a) and (c), 0.3 μm (e) and (f).

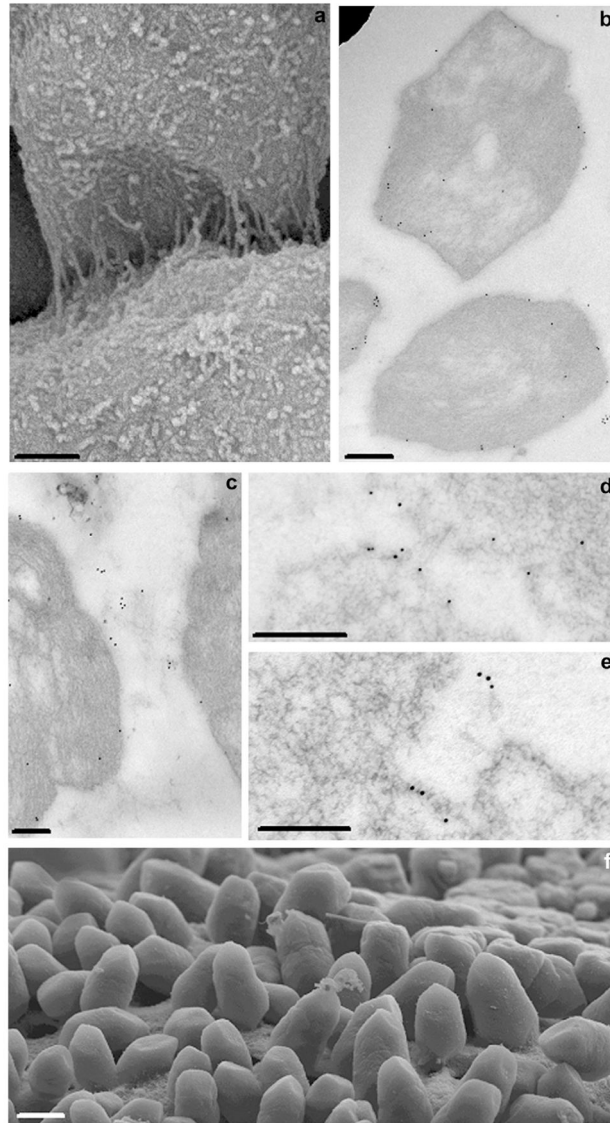


Fig 6.

Interconnections of otoconia shown by SEM and immunogold TEM of otolin. (a) SEM image of adjacent otoconia showing dense fibrillar interconnections. The surface of PN3 day otoconia is covered with meandering fibrils whereas adjacent otoconia are interconnected by thin, tight fibrils; (b) and (c) images of ED18 mouse otoconia; (b) shows gold particles close to surface or within subsurface layer; (c) shows gold particles labeling interotoconial fibrils. (d) and (e) are images of young adult otoconia; (d) gold labeling of corresponding surfaces of otoconia; (e) pair of triplets of gold particles corresponding to interconnecting fibrils; (f) SEM image of otoconial layer of two-year-old mouse. Otoconial surface is denuded and otoconia are arranged in vertical orientation with tips projecting into endolymphatic lumen. Only lower tips of otoconia are loosely attached to the remnants of the fibrogelatinous matrix. Bars = 0.35 μm (a), 0.25 μm (b), 0.35 μm (c), 0.23 μm (d), 0.5 μm (e), 5.5 μm (f).